Article

A Novel Method for Friction Coefficient Calculation in Metal Sheet Forming of Axis-Symmetric Deep Drawing Parts

Jiansheng Xia [1,2,*], **Jun Zhao [1,*]**, **Shasha Dou [2]** and **Xing Shen [2]**

1   College of Mechanical Engineering, Yanshan University, Qinhuangdao 066004, China
2   College of Mechanical Engineering, Yancheng Institute of Technology, Yancheng 224051, China; lisadou@ycit.edu.cn (S.D.); lisadou2009@gmail.com (X.S.)
*   Correspondence: xiajs@ycit.edu.cn (J.X.); zhaojun@ysu.edu.cn (J.Z.); Tel.: +86-15861988970 (J.X.); +86-335-8074648 (J.Z.)

Abstract: Friction is one of the important factors in sheet metal forming. It greatly affects dynamic behaviors of metal sheets and stress and strain distributions in the metal sheets. In this study, deformation characteristics, stress–strain distribution, and change law of symmetrical parts in the process of deep drawing are analyzed using a new theoretical model based on the plastic flow law and partitioning the forming area. In the model, the least-square method is used to linearize the friction coefficient in nonlinear problems and reverse the calculation of friction coefficients to interpret the friction coefficient. To evaluate the model, the friction coefficient in sheet metal drawing of axis-symmetric deep drawing parts under various friction conditions was measured using a self-developed measuring system. The comparison between the experimental results and the calculation using the model shows a good agreement. The results show that the drawing force increases with the increase in punch depth; the friction coefficient decreases with the rise in punch depth. The friction coefficient obtained by fitting is relatively stable, and the average error is less than 3%. Using the friction coefficient model in finite element simulation analysis, it shows that the thickness and blank shape errors are less than 5%. The novel method studied in this paper shows great significance in support for theoretical research, numerical simulation research, and sheet metal stamping performance evaluation.

Keywords: friction coefficients; calculation method; finite element simulation; sheet forming; symmetrical part

1. Introduction

Sheet metal forming by plastic processing requires fewer consumables, and has high productivity and low cost. The products have light weight and good internal organization performance, which are widely used in aircraft, automobile, motor and electrical appliances, instruments, and many other industries. Therefore, the plastic forming processing of metal materials plays a significant role in national economic construction and is an important method in manufacturing [1]. Axisymmetric parts are often found in sheet metal forming, which is a kind of plastic processing. In the stamping production of national industrial departments, stamping and drawing technology are always significant [2].

Stamping forming involves many factors such as sheet properties, blank holder force, and friction. The selection of these process parameters influences the results of sheet forming greatly. For the process parameters, the fluctuation of the friction coefficient has a much greater impact on the process than the material properties and other process parameters. The main reason is the lack of understanding of friction problems in plastic forming and simply using the Coulomb friction law compared with other influencing factors. Thus, the effect of friction in sheet metal forming is simplified. Meanwhile, the lubrication conditions fluctuate greatly and change frequently in the process of sheet metal plastic forming, and result in great influences and complex situations.

There has been little progress on modeling of friction in sheet metal plastic forming in the past years, because there are too many unknowns in the friction mechanism and friction process in the stamping process. The dynamic friction process in the stamping process is very complex [3]. Many research efforts have been made. Kudo and Azushima [4] proved that the friction coefficient depended on the contact pressure using a transparent quartz mold's thin-plate stretching device. Dohda and Wang [5] conducted a series of friction and wear tests with rolling friction and a wear tester. Their studies showed the influence of average speed in the contact area and the relative sliding speed between the roller and the workpiece on the friction and wear during deformation. The sliding speed had a particular influence on the friction coefficient. Ma et al. [6] established a roughness model in metal forming. Their results showed that the contact-specific area increased with the increase in nominal pressure, and the relative sliding between die and plate could increase the contact-specific area. Wilson et al. [7] established friction models for different lubrication conditions by internal interface variables such as average lubricating oil film thickness, plate roughness and die roughness, contact pressure and sliding speed. Compared with the Amontons Coulomb friction coefficient model, the accuracy in the calculation was increased by about 10%. Comstock et al. [8] conducted sliding tests on a 270 MPa tensile strength coated plate and proposed a new friction coefficient model described by polynomial expression, including load and sliding length variables. Hildenbrand et al. [9] proposed a nonlinear friction coefficient model to improve the friction modeling in stamping simulation with consideration of the variables of contact pressure, sliding speed and friction work on the friction coefficient. Through the analysis of numerical simulation and experimental results compared with the constants of Coulomb law, it was found that the nonlinear friction law has a better prediction on thickness, fracture, and punch force. Hashimoto et al. [10] considered the contact pressure and sliding length in predicting the friction coefficient and proved that the nonlinear model was more accurate than the Coulomb friction law in finite element analysis through experiments. K. Dohda et al. [11] developed a new nonlinear friction coefficient model, considering the effects of contact pressure, velocity, sliding length, and friction work. It showed that the friction coefficient decreased with the increase in sliding length. Bhushan [12] believed that in many metal pairs under high load, the friction coefficient decreased with the increase in load and the growth of surface roughness. It was thought that the generation of a lot of wear debris was the main reason for the reduction in friction. Chow. et al. [13] studied the effects of average load and sliding speed on the friction and wear properties between an aluminum disk and stainless-steel pin. They found that the friction coefficient of metals increased with the increase in sliding velocity, and the wear rate increased with the growth in sliding speed and average load.

Based on the nonlinear least-square curve-fitting principle, the friction coefficient is studied for axisymmetric deep drawing parts and a new model is developed. The friction coefficients in sheet metal forming of an axisymmetric deep drawing part were measured with different material parameters by self-developed measuring equipment and compared with the calculations using the model. Finally, the friction model is verified using finite element simulations and the experimental results.

2. Theory and Methods

2.1. Theoretical Analysis

A cylindrical part is one of the typical axisymmetric parts, such as drawing dies. A drawing die consists of a punch, a die, and a blank holder, as shown in Figure 1. In the drawing die, blanking clearance is slightly greater than the blank thickness, which results in a nonstraight wall of the part's sidewall. Therefore, the cylindrical symmetrical part can be treated as a conical part with a small taper. According to the stress and strain distribution of deep axis-symmetric drawing, the deformation area is divided into several parts [14]: barrel bottom area (zone 1-lime): $0 \leq \xi \leq R_A$, punch fillet area (zone 2-blue): $R_A \leq \xi \leq R_B$, sidewall area (zone 3-green): $R_B \leq \xi \leq R_C$, punch fillet area (zone 4-rose):$R_C \leq \xi \leq R_D$ and flange area (zone 5-gold): $R_D \leq \xi \leq R$.
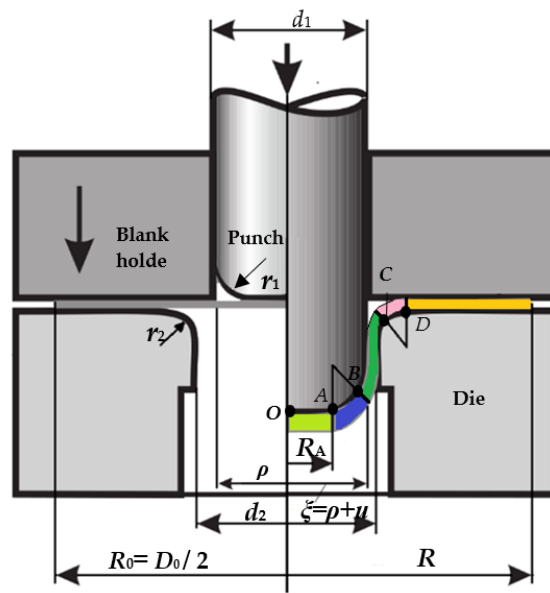
Figure 1. Drawing diagram of symmetrical cylindrical parts.

There is contact friction between the workpiece and the blank holder, punch and die in zone 4 and zone 5 for drawing symmetric cylindrical parts. In previous studies, the friction of the flange part used to be simplified as the contact friction between the flange part and the die surface, and only the friction caused by blank holder force was considered [15]. There is friction on the outer periphery of the flange, i.e., the single-sided friction on the unit arc length. In the analysis of die fillet, the Euler formula is often used as an approximation. Hence, a simplified model is shown in Figure 2. Friction in the upper surfaces in zones 4 and 5 are considered based on the perspective of the axial external force balance of the workpiece.
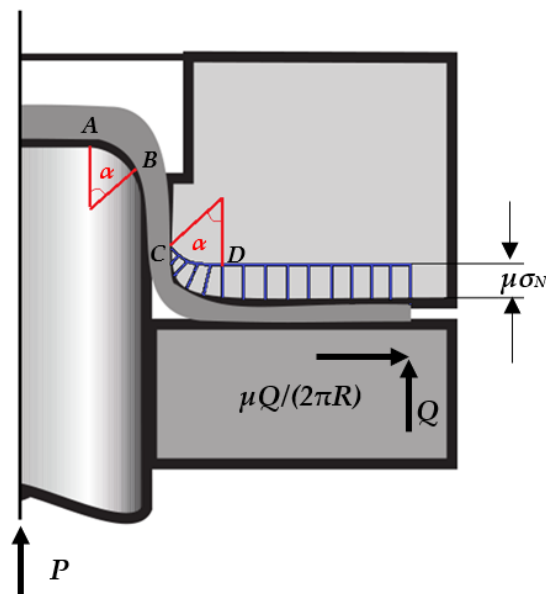
Figure 2. Simplification of symmetric friction stress during drawing.

As shown in Figure 2, the friction stress on the upper surface of zone 5 is evenly distributed.

$$\tau_5 = \mu\sigma_N \tag{1}$$

where τ_5 is friction stress of zone 5; μ is friction coefficient; σ_N is the normal contact stress uniformly distributed on the upper surface of zone 5. The stress distribution on zone 4 (τ_4) has the following two boundary conditions: $\tau_4|_{\xi=R_C} = 0$ and $\tau_4|_{\xi=R_D} = \mu\sigma_N$, and the distribution is

$$\tau_4 = \mu\sigma_N \cdot \frac{\sin(\alpha - \theta)}{\sin\alpha} \qquad 0 \leq \theta \leq \alpha \tag{2}$$

where σ_N can be

$$\sigma_N = \frac{P+Q}{\pi r_{20}^2} \cdot K(\alpha) \tag{3}$$

$$K(\alpha) = \frac{r_{20}^2}{R^2 - R_D^2 + \alpha r_{20}R_D - \frac{2}{3}r_{20}^2(1 - \cos\alpha)} \tag{4}$$

Taking the relationship between the instantaneous radial coordinates of the mass point in each deformation area [16], and the punch stroke and the original radial coordinates, $\xi = \xi(\rho, h)$:

$$\begin{cases} \xi = \rho & 0 \leq \xi \leq R_A \\[2mm] \xi = R_A + r_{10}\sin\theta \\ \rho^2 = R_A^2 + 2r_{10}[R_A\theta - r_{10}(\cos\theta - 1)] & R_A \leq \xi \leq R_B(0 \leq \theta \leq \alpha) \\[2mm] \rho^2 = R_A^2 + 2r_{10}[R_A\alpha - r_{10}(\cos\alpha - 1)] + \frac{\xi^2 - R_B^2}{\cos\alpha} & R_B \leq \xi \leq R_C \\[2mm] \xi = R_D - r_{20}\sin\theta \\ R_0^2 - \rho^2 = R^2 - R_D^2 + 2r_{20}[R_D\theta + r_{20}(\cos\theta - 1)] & R_C \leq \xi \leq R_D(0 \leq \theta \leq \alpha) \\[2mm] R_0^2 - \rho^2 = R^2 - \xi^2 & R_D \leq \xi \leq R \end{cases} \tag{5}$$

2.2. Basic Equations

(1) Geometric equation

$$\varepsilon_r = \ln\left[\sqrt{1 + \left(\frac{\partial w}{\partial\xi}\right)^2} \cdot \frac{\partial\xi}{\partial\rho}\right] \tag{6}$$

$$\varepsilon_\theta = \ln\frac{\xi}{\rho} \tag{7}$$

where, ρ is the original coordinate of a point before deformation. When the drawing height is h; w is the instantaneous axial coordinate of the point and ξ is the instantaneous radial coordinate.

(2) Flow equation

$$\frac{\dot{\varepsilon}_r}{\sigma_r - \frac{r}{1+r}\sigma_\theta} = \frac{\dot{\varepsilon}_\theta}{\sigma_\theta - \frac{r}{1+r}\sigma_r} = \frac{\dot{\varepsilon}}{\sigma} \tag{8}$$

where r is the thickness anisotropy coefficient; σ, ε and $\dot{\varepsilon}$ are the equivalent stress, equivalent strain, and equivalent strain rate, respectively.

(3) Constitutive equation

$$\sigma = A \cdot \varepsilon^n \tag{9}$$

where A is material coefficient; n is the hardening index.

(4) Energy equation

$$\int_S T_i \cdot \dot{u}_i dS = \int_S \sigma_{ij} \cdot \dot{\varepsilon}_{ij} dV \tag{10}$$

where T_i is the join force on point i; $\dot{u}_i$ is the displacement in force direction. The left side of the equation is the work done by the external load per unit time and the work consumed

by the friction force of the contact surface in zone 4 and zone 5 per unit time. The right side of the equation is the plastic deformation work per unit time in zones 3, 4, and 5 and bending deformation work per unit time.

(5) Equivalent strain The equivalent strain is calculated by assuming that the area is unchanged and the geometric equation of symmetrical parts is:

$$
\varepsilon = \begin{cases}
0 & 0 \leq \xi \leq R_A \\[2mm]
\omega \ln \dfrac{R_A^2 + 2r_{10}[R_A\theta - r_{10}(\cos\theta - 1)]}{(R_A + r_{10}\sin\theta)^2} & R_A \leq \xi \leq R_B, (0 \leq \theta \leq \alpha) \\[2mm]
\omega \ln\left\{ \dfrac{1}{\xi^2}\left[R_A^2 + 2r_{10}(R_A\alpha + r_{10}(1-\cos\alpha)) \right] + \dfrac{1}{\cos\alpha}\left(1 - \dfrac{R_B^2}{\xi^2}\right) \right\} & R_B \leq \xi \leq R_C \\[2mm]
\omega \ln \dfrac{R_0^2 + R_D^2 - R^2 - 2r_{20}[R_D\theta + r_{20}(\cos\theta - 1)]}{(R_D - r_{20}\sin\theta)^2} & R_C \leq \xi \leq R_D, (0 \leq \theta \leq \alpha) \\[2mm]
\omega \ln\left(1 + \dfrac{R_0^2 - R^2}{\xi^2}\right) & R_D \leq \xi \leq R
\end{cases}
\tag{11}
$$

(6) Flow velocity The radial displacement velocity of particles in each deformation area is:

$$
\dot{u} = \begin{cases}
0 & 0 \leq \xi \leq R_B \\[2mm]
-\dfrac{\xi^2 - R_B^2}{2\xi} \cdot \dfrac{\sin\alpha\cos\alpha}{R_C - R_B} \cdot \dot{v} & R_B \leq \xi \leq R_C \\[2mm]
-\dfrac{1}{2}\sin\alpha(R_B + R_C) \cdot \dfrac{\cos\theta}{R_D - r_{20}\sin\theta} \cdot \dot{v} & R_C \leq \xi \leq R_D, (0 \leq \theta \leq \alpha) \\[2mm]
-\dfrac{1}{2\xi}\sin\alpha(R_B + R_C) \cdot \dot{v} & R_D \leq \xi \leq R
\end{cases}
\tag{12}
$$

In the drawing process of symmetrical parts, the absolute flow velocity of particles on each friction surface is: $\dot{u}_f = \dot{u}/\cos\theta$ in zone 4, $\dot{\varepsilon} = 2\omega|\dot{u}|/\xi$ in zone 5, the equivalent strain rate of particles in different deformation zones is deduced as:

$$
\dot{\varepsilon} = \begin{cases}
0 & 0 \leq \xi \leq R_B \\[2mm]
\omega \dfrac{\xi^2 - R_B^2}{\xi^2} \cdot \dfrac{\sin\alpha\cos\alpha}{R_C - R_B} \cdot \dot{v} & R_B \leq \xi \leq R_C \\[2mm]
\omega \sin\alpha(R_B + R_C) \cdot \dfrac{\cos\theta}{(R_D - r_{20}\sin\theta)^2} \cdot \dot{v} & R_C \leq \xi \leq R_D, (0 \leq \theta \leq \alpha) \\[2mm]
\omega \dfrac{1}{\xi^2}\sin\alpha(R_B + R_C) \cdot \dot{v} & R_D \leq \xi \leq R
\end{cases}
\tag{13}
$$

2.3. Axisymmetric Drawing Analysis

Based on the above results, $\sigma_{ij}\dot{\varepsilon}_{ij} = \sigma \cdot \dot{\varepsilon}$, the expression of the drawing force of symmetrical cylindrical parts can be obtained as:

$$
P = \int_{F_f} \tau \frac{|\dot{u}|}{\dot{v}} \cdot \frac{dF_f}{\cos\theta} + \int_V \sigma \frac{|\dot{u}|}{\dot{v}} \cdot \frac{dV}{\xi} + \sum M_i \frac{\dot{\phi}_i}{\dot{v}}
\tag{14}
$$

where $\dot{u}$ is the radial displacement velocity; F_f is the friction contact surface; $\dot{v}$ is the punch velocity; $\dot{\phi}$ is the bending angular velocity.

Substituting Equations (1), (4), and (12) into (14), the drawing force stroke curve is obtained.

$$
P = \frac{C(\alpha)}{1 - \mu K_c(\alpha) K(\alpha, \mu)} [\mu Q F(\alpha) + 2\omega I(\alpha) + J(\alpha)]
\tag{15}
$$

$$\begin{cases}
C(\alpha) = \pi t_0 (R_B + R_C) \sin \alpha \\[4pt]
F(\alpha) = \dfrac{1}{2\pi t_0 R} \left[1 + \dfrac{2R}{r_{20}^2} \left(\dfrac{\sin \alpha}{1 + \cos \alpha} r_{20} + R - R_D \right) \cdot K(\alpha) \right] \\[4pt]
I(\alpha) = I'(\alpha) + I''(\alpha) + I'''(\alpha) \\[4pt]
I'(\alpha) = \displaystyle\int_{R_B}^{R_C} \sigma_3 \dfrac{\xi^2 - R_B^2}{R_C^2 - R_B^2} \cdot \dfrac{d\xi}{\xi} \\[4pt]
I''(\alpha) = \displaystyle\int_{0}^{\alpha} \sigma_4 \dfrac{r_{20} \cos \alpha}{R_D - r_{20} \sin \theta} d\theta \\[4pt]
I'''(\alpha) = \displaystyle\int_{R_D}^{R} \sigma_5 \cdot \dfrac{d\xi}{\xi} \\[4pt]
J(\alpha) = \dfrac{t_0}{4 r_{20}} \left[G(\alpha) \cdot \left(\dfrac{R_B}{R_C} \sigma_{3B} + \sigma_{4C} \right) + \sigma_{5D} \right] \\[4pt]
G(\alpha) = \dfrac{2 r_{20} R_C}{R_C^2 - R_B^2} \operatorname{ctg}\alpha \cdot \cos \alpha \\[4pt]
K_1(\alpha) = \dfrac{\sin \alpha}{r_{20}^2} (R_B + R_C) \cdot \left(\dfrac{\sin \alpha}{1 + \cos \alpha} r_{20} + R - R_C \right) \cdot K(\alpha) \\[4pt]
K(\alpha) = \dfrac{r_{20}^2}{R^2 - R_D^2 + r_{20} R_D \alpha - \frac{2}{3} r_{20}^2 (1 - \cos \alpha)}
\end{cases} \tag{16}$$

2.4. Algorithm for Friction Coefficient Calculation

The friction coefficient can be calculated when the data and plate parameters are known. The theoretical drawing force–stroke curve calculated by the analytical formula (15) and (16) is fitted with the measured drawing force–stroke curve. According to references [17], the drawing friction coefficient can be expressed as:

$$\mu = \frac{P - \mu Q C(h) F(h) + C(h)[2\omega I(h) + J(h)]}{P \cdot K_1(h)} \tag{17}$$

The relevant parameters can be measured. According to the least-square method, a new parameter function can be the square sum of the residuals between the measured and theoretical calculated values.

$$F_{obj}(\mu) = \sum_{i=1}^{N} [P_i - P(\mu, Q_i, h_i)]^2, \ (i = 1, 2, 3, \ldots, N) \tag{18}$$

The minimum point of the Equation (18) is the solution, so the friction coefficient can be obtained as:

$$\mu = \frac{\displaystyle\sum_{i=1}^{N} [P_i - T(h_i)] \cdot [P_i \cdot K_1(h_i) + Q_i S(h_i)]}{\displaystyle\sum_{i=1}^{N} [P_i \cdot K_1(h_i) + Q_i \cdot S(h_i)]^2} \tag{19}$$

3. Materials and Experiment

3.1. Materials

Two materials of Al-5754 (Southwest Aluminum (Kunshan) Co., Ltd., Kunshan, China) and SPCC (Shanghai Baosteel Group, Shanghai, China) are used in the experiments, where the thickness of samples is 1mm. The material composition is shown in Tables 1 and 2. The samples are stretched from each plate at 0°, 45°, and 90° to the rolling direction performed by tensile tests. The arithmetic average of the test results of three samples is taken in each direction. The final plate performance parameters are calculated according to the weighted average of the performance test results in three directions. The results are shown in Table 3.

Table 1. Chemical composition of Al-5754 sheet.

Components	Si	Fe	Cu	Mn	Mg	Cr	Zn	Ti	Al
%	0.40	0.40	0.10	0.5	2.6~3.6	0.30	0.20	0.15	Bal.

Table 2. Chemical composition of two kinds of steel sheets SPCC.

Components	C	Si	Mn	P	S	Ni	Cr	Cu
%	≤0.12	-	≤0.12	≤0.04	≤0.045	-	-	-

Table 3. Performance parameters of plates.

Sheet No.	Sampling Direction	Yield Strength σ_s (MPa)	Tensile Strength σ_b (MPa)	Uniform Elongation δ_u (%)	Strength Coefficient B (MPa)	Hardening Exponent n	Thickness Anisotropy Coefficient r
SPCC	0°	205.187	277.652	24.742	484.93	0.223	2.387
	45°	216.582	291.925	25.468	507.56	0.220	1.498
	90°	215.593	283.429	26.810	499.45	0.229	2.143
	Ave.	212.454	284.335	25.673	497.31	0.224	2.009
Al-5754	0°	112.31	212.64	22.361	407.96	0.247	0.748
	45°	109.31	215.63	24.245	415.85	0.278	0.845
	90°	108.94	213.37	24.157	424.61	0.273	0.794
	Ave.	110.187	213.88	23.588	416.14	0.266	0.796

3.2. Friction Coefficient Measurement

With the material parameters, the friction coefficient measurement principle (see Figure 3). The calculated friction model is imported into the finite element software for simulation analysis, so as to improve simulation accuracy. The friction coefficient is measured using a self-developed punching system and equipment (see Figure 4a). It is lubricated with butter, which is evenly applied on the surface of the sheet. The diameter of blank T = 140 mm; punch diameter *d* = 70 mm; die diameter *D* = 71 mm; punch fillet radius *r* = 10 mm; die fillet radius *R* = 6 mm. According to the nonlinear friction coefficient algorithm of symmetrical plate deduced above, the relevant tensile test data, and input the values of tensile force (*P*), stroke (*H*) and blank holder force (*Q*) of each test, the friction coefficient is calculated. The collected data are input into the programmed MATLAB program to obtain the friction coefficient of sheet metal stamping. Taking the performance parameters of each experimental plate, the friction coefficient under the given conditions is calculated. Three experiments for each group were undertaken, and the average value calculated. The drawing force and punch depth curve is calculated with the known material performance parameters and die geometric parameters. The calculation results of the friction coefficient of each plate are shown in Figure 4b. The relationship curve between drawing force and stamping depth is shown in Figure 5. The friction coefficient and punch depth curve is shown in Figure 6.
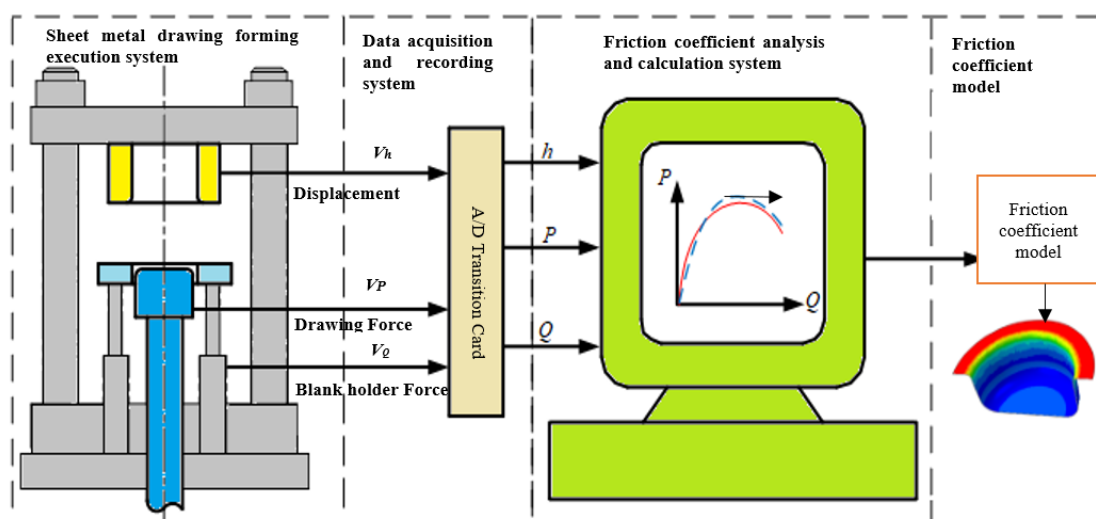
Figure 3. Schematic diagram of friction coefficient measurement system.
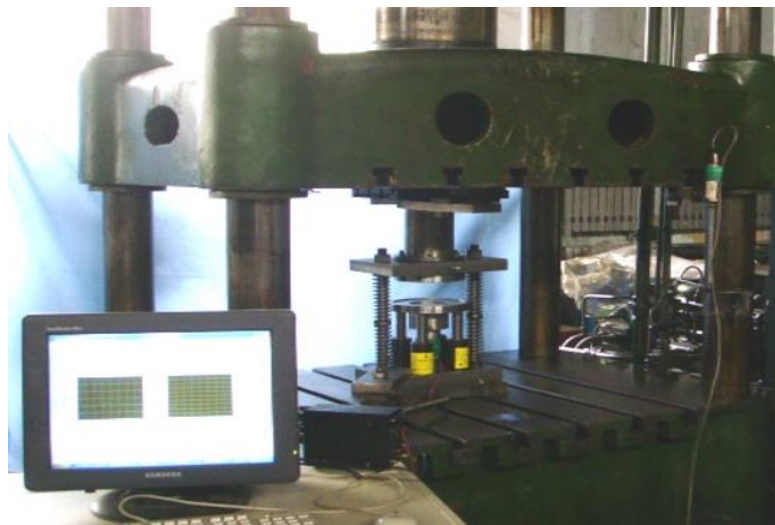
(**a**)
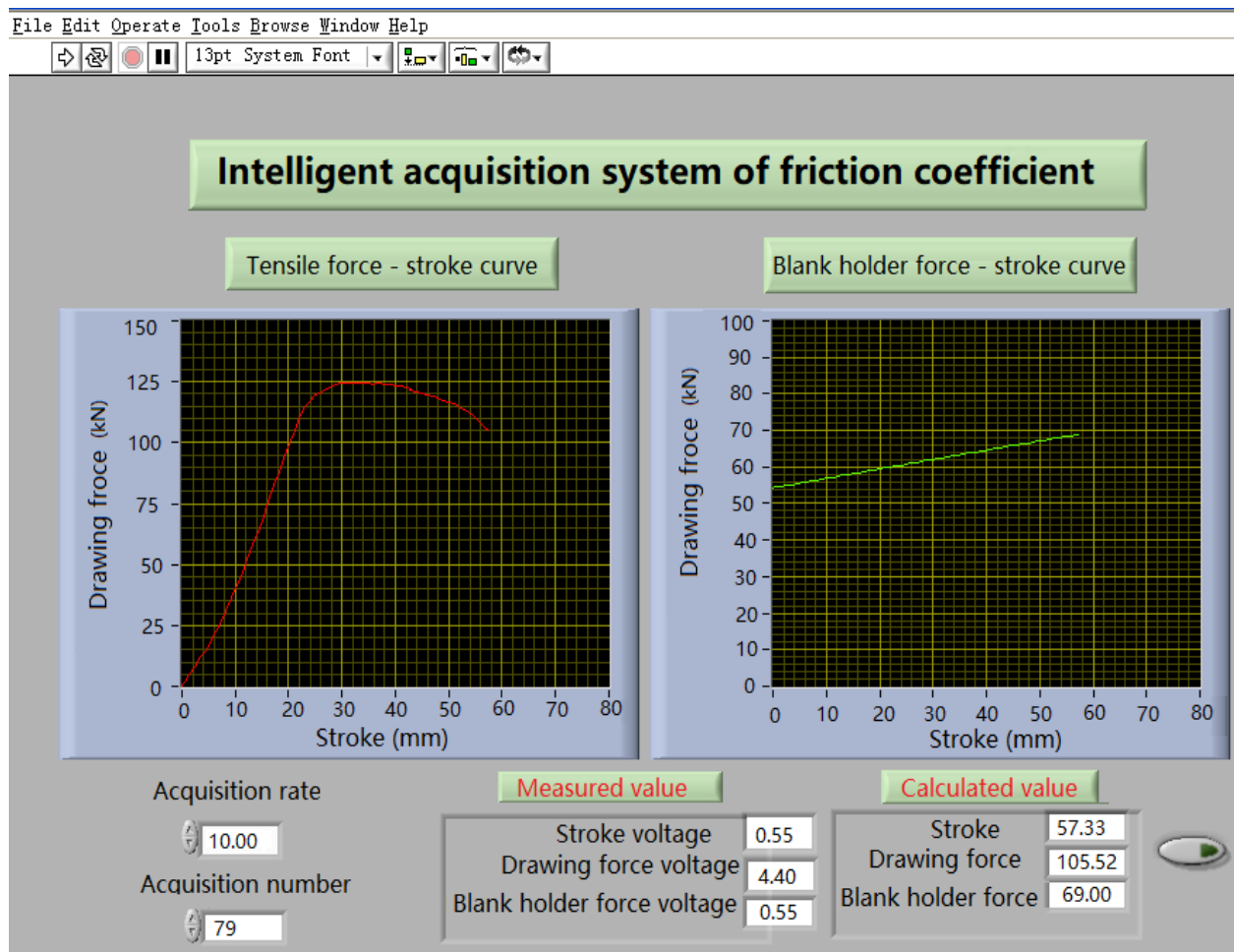
(**b**)

Figure 4. Friction coefficient measuring equipment and algorithm. (**a**) Friction coefficient measuring equipment; (**b**) Friction coefficient measurement system.
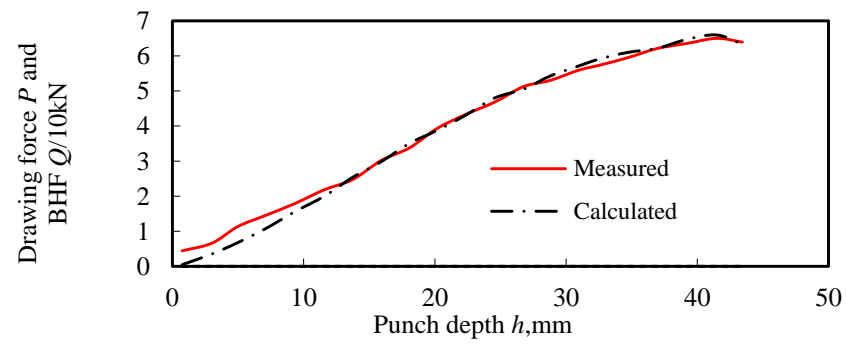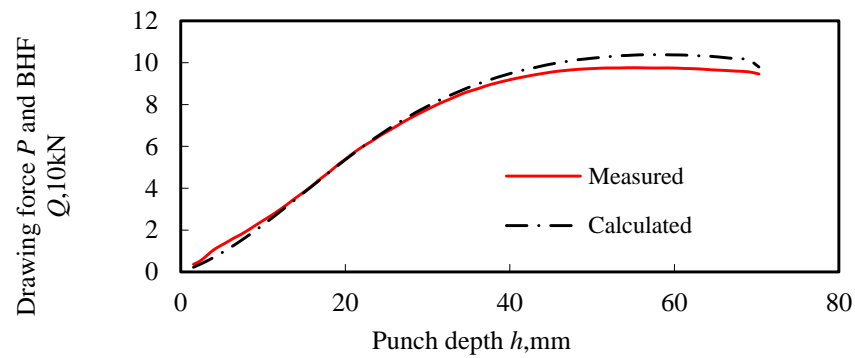
Figure 5. Drawing force and Punch depth curve. (**a**) SPCC steel; (**b**) Al-5754.
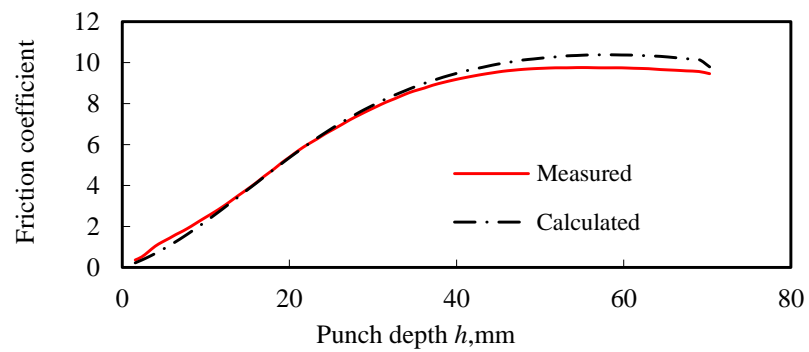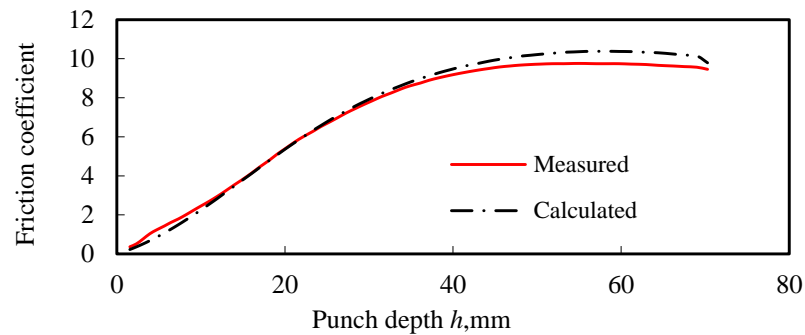
Figure 6. Friction coefficient and Punch depth curve. (**a**) SPCC steel; (**b**) Al-5754.

As shown in Figure 6, the theoretical drawing force–punch depth curve is matched with the measured curve relatively well. Because the friction model is established for the middle and late stages of deep drawing, the friction mainly acts on the outer edge of the flange, and the friction is almost evenly distributed in the initial phase of deep drawing. If the model established in the middle and late stages is used to measure the friction coefficient in the initial stage of deep drawing, the result will be too large. When the drawing depth is about 20 mm, it can be seen that the friction coefficient obtained by fitting is a relatively stable value. At the same time, in the initial stage of deep drawing, due to a certain adhesion between punch and plate, it does not fully enter the sliding friction state. These also cause a large measured friction coefficient.

3.3. Error Analysis

The friction coefficient is calculated according to the given material parameters. The results show that the theoretical drawing force is in good agreement with the measured drawing force curve. Because the curve measured contains many data points, the friction coefficient is brought into the formula to obtain the same number of theoretical drawing force data points. Figure 7 shows the relative error curves between the calculated drawing force and the measured drawing force of some plates under different lubrication conditions. The coincidence degree of the two curves is explained by comparing the two groups of data.

(**a**)

(**b**)
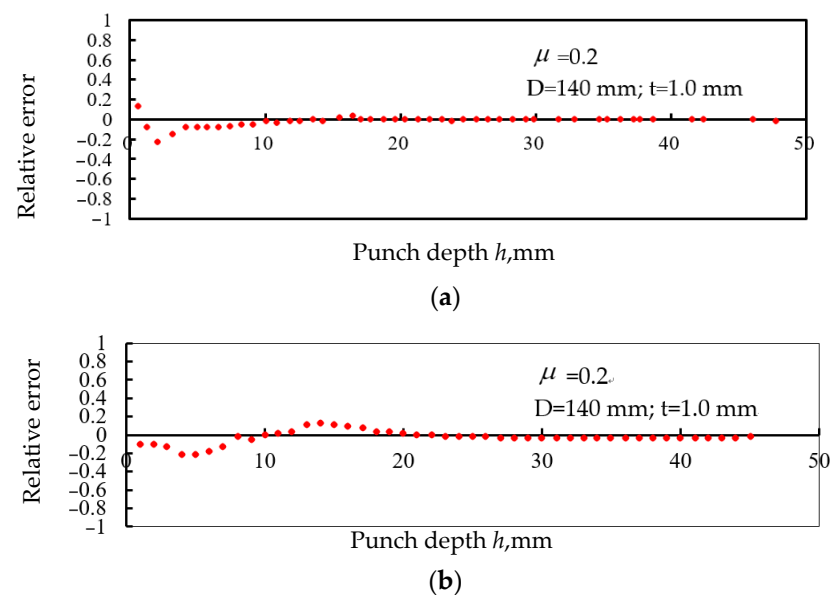
Figure 7. The relative error of calculation and measurement drawing Force. (**a**) SPCC steel; (**b**) Al-5754.

4. Results and Discussion

The friction in processing of Al-5754 is simulated using the friction model developed. The ABAQUS/Explicit module is adopted. The dimensions are shown in Figure 8a, the three-dimensional model is shown in Figure 8b. Because the cylinder is symmetrical, the 1/4 model is used for analysis effectively. Using the user-defined material subroutine interface, UMAT, provided by ABAQUS software, the required constitutive model has been redeveloped in the finite element software for numerical simulation. The friction model is defined by the keyword "*FRICTION" in the user subroutine, which is used to introduce the friction characteristics into the surface contact model to control the surface contact behavior. The tool type was defined as a rigid body element of R3D4, while the metal type is a deformed body element of C3D8R, divided with the grid control attribute into 2895 grid elements by the quadrilateral sweep method according to the single-precision offset control method.
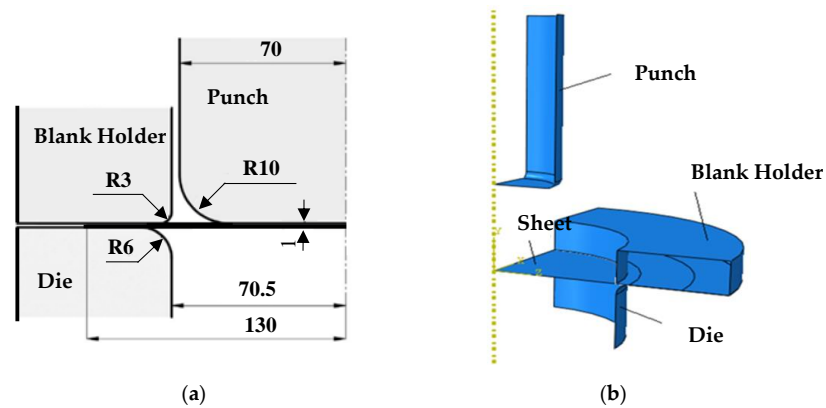
Figure 8. Schematic diagram of drawing parameters of cylindrical parts. (**a**) Parametric dimensions of symmetrical part and tools; (**b**) Finite element 3d model.

Under a blank holder force of 2.0 MPa, using the friction coefficient model with a constant friction coefficient ($\mu = 0.2$), finite element simulation and analysis of the wall thickness are carried out. The simulation results are compared to the experimental results as shown in Figures 9 and 10. It shows the wall thickness distribution at other parts of the cylinder wall at different drawing heights for $\mu = 0.2$ and the friction coefficient model. It shows that the thickness changes with the drawing. The flange part becomes thicker and the fillets of die and punch become thinner. The fillet of punch is the worst part. When the stroke increases, the bottom area becomes thinner.

(**a**)

(**b**)

(**c**)
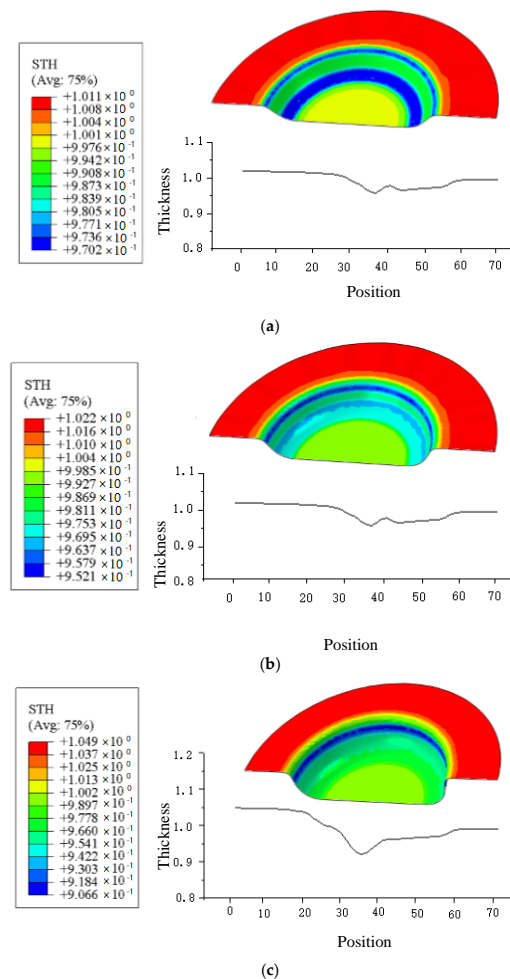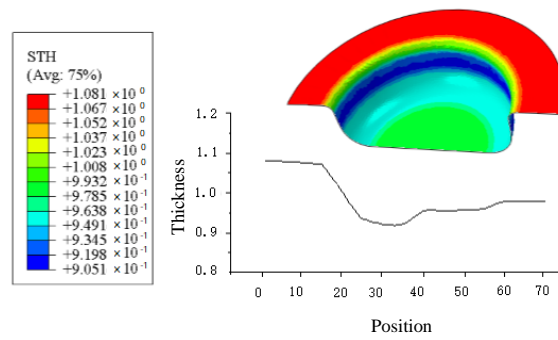
Figure 9. *Cont*.

(d)
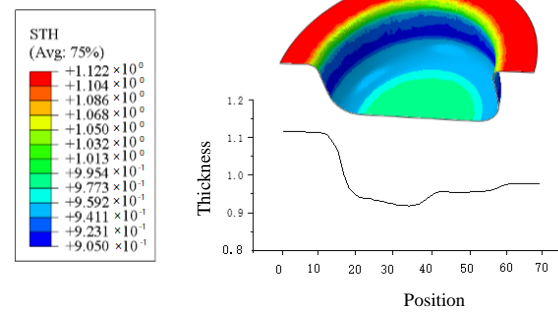
(e)

Figure 9. Wall thickness location points and wall thickness distribution under constant friction coefficient (μ = 0.2); (**a**) h1 = 10 mm; (**b**) h2 = 15 mm; (**c**) h3 = 20 mm (**d**) h4 = 25 mm; (**e**) h5 = 30 mm.

(**a**)

Figure 10. *Cont.*

(b)

(c)

(d)
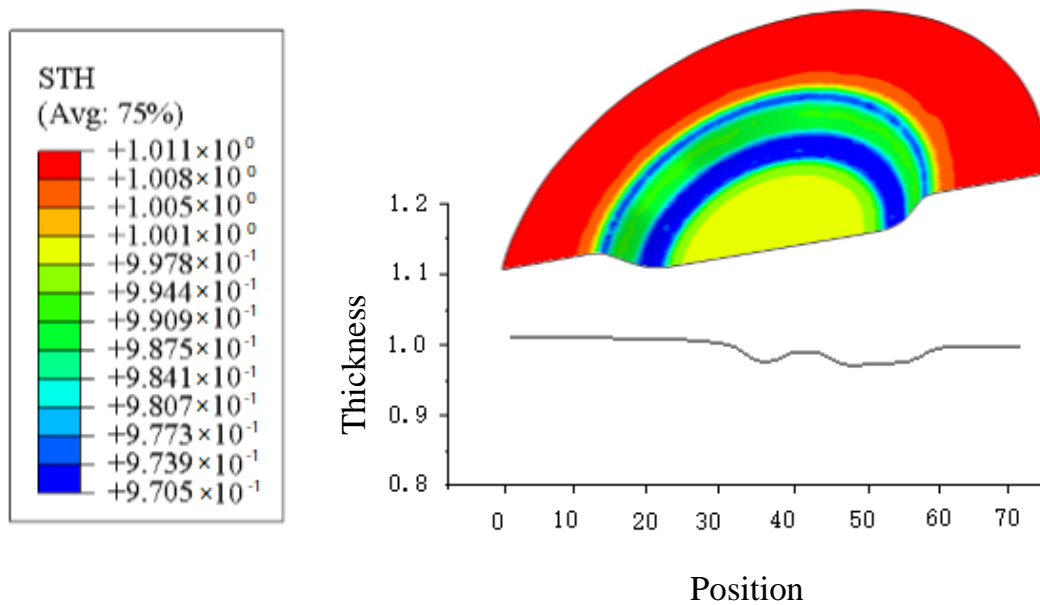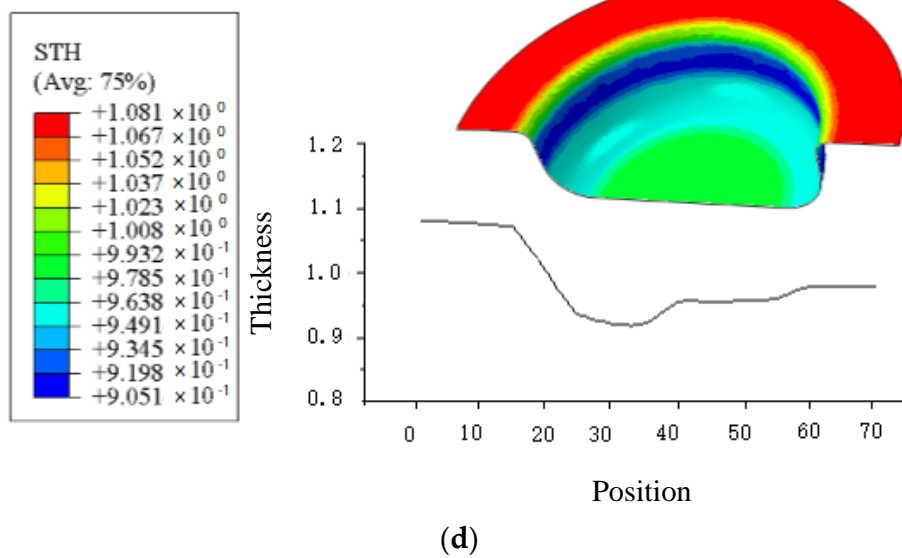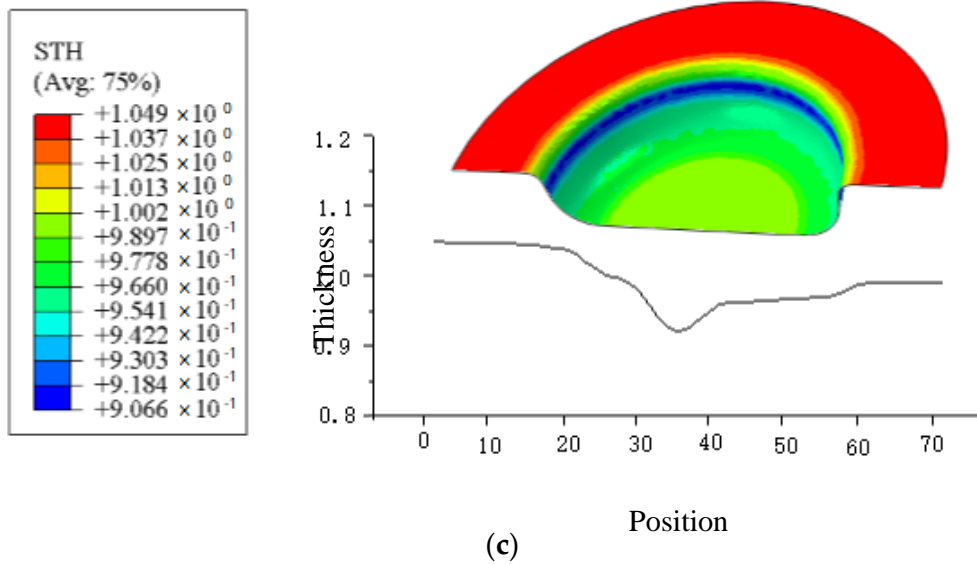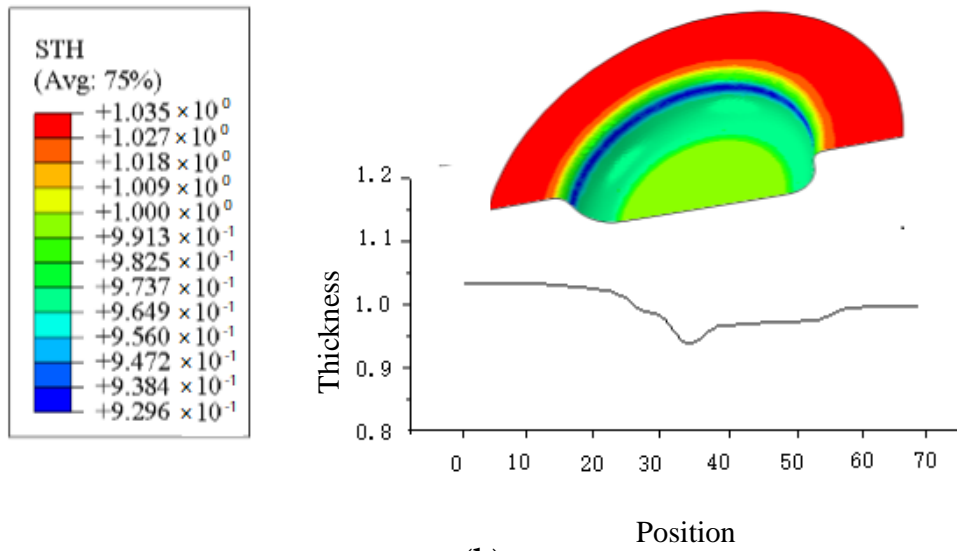
Figure 10. *Cont.*
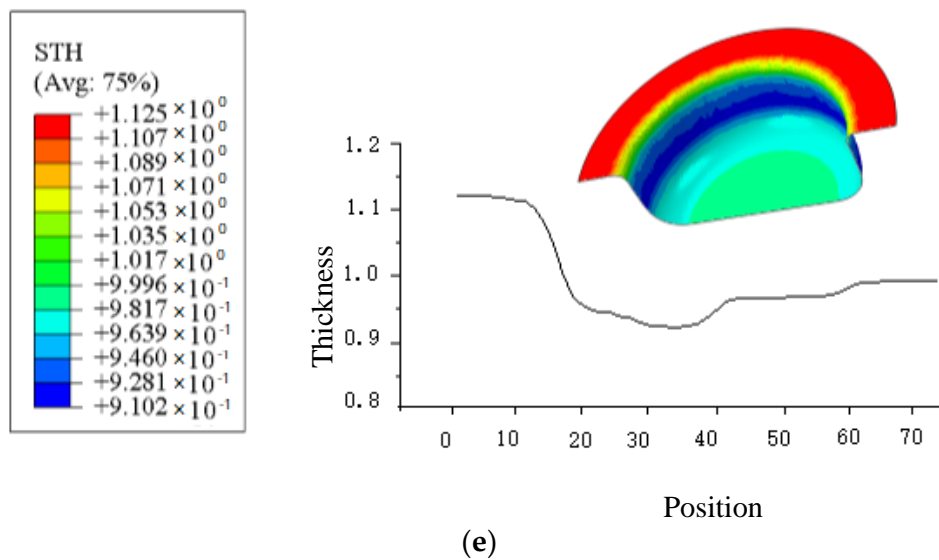
Figure 10. Wall thickness location points and wall thickness distribution under variable friction coefficient model, (**a**) h1 = 10 mm; (**b**) h2 = 15 mm; (**c**) h3 = 20 mm; (**d**) h4 = 25 mm; (**e**) h5 = 30 mm.

To compare the variation of the measured thickness of the parts, the wall thickness at eight position points (see Figure 11) in five different cylinder areas is taken for the measurement. The simulated and measured wall thickness are shown in Table 4. For the variation law of part wall thickness, the thickness of the friction model is closer to the actual value. It shows:

(1) The diameter of the flange area (zone 1) becomes smaller when deformed, resulting in the extrusion of the material and the thickness increase. The maximum thickness is 1.114 mm.

(2) The material is continuously pulled into the die in the die's fillet area (zone 2) and becomes a part of the straight wall. The material is plastically deformed and the wall thickness is thinned.

(3) This area of the cylinder wall (zone 3) plays a role in transmitting the drawing force to the drawing material, with a small amount of radial elongation, resulting in the phenomenon of thickness thinning.

(4) The punch fillet area (zone 4) is the transition area of the cylinder wall. The material is subjected to the dual action of the fillet surface's compressive stress and tensile stress. The thinnest part of the whole part has low strength and a minimum of 0.831 mm.

(5) At the beginning, the area at the bottom (zone 5) is pulled into the die and maintains a plane state. The friction at the fillet of the punch limits the outflow of materials. It is only subject to the compressive stress of the punch, with small deformation and slightly reduced thickness.

Table 4. Wall thickness distribution of parts.

Positions	Actual Value (mm)	μ=0.2 (mm)	Friction Coefficient Model (mm)
1	1.108	1.078 (Error: −2.70%)	1.085 (Error: −2.07%)
2	1.071	1.045 (Error: −2.43%)	1.060 (Error: −1.03%)
3	0.925	0.903 (Error: −2.38%)	0.938 (Error: 1.41%)
4	0.892	0.823 (Error: −7.74%)	0.908 (Error: 1.79%)
5	0.875	0.837 (Error: −4.34%)	0.852 (Error: −2.63%)
6	0.843	0.807 (Error: −2.47%)	0.831 (Error: −1.42%)
7	0.851	0.815 (Error: −4.23%)	0.835 (Error: −1.88%)
8	0.845	0.863 (Error: 2.138%)	0.856 (Error: 1.30%)
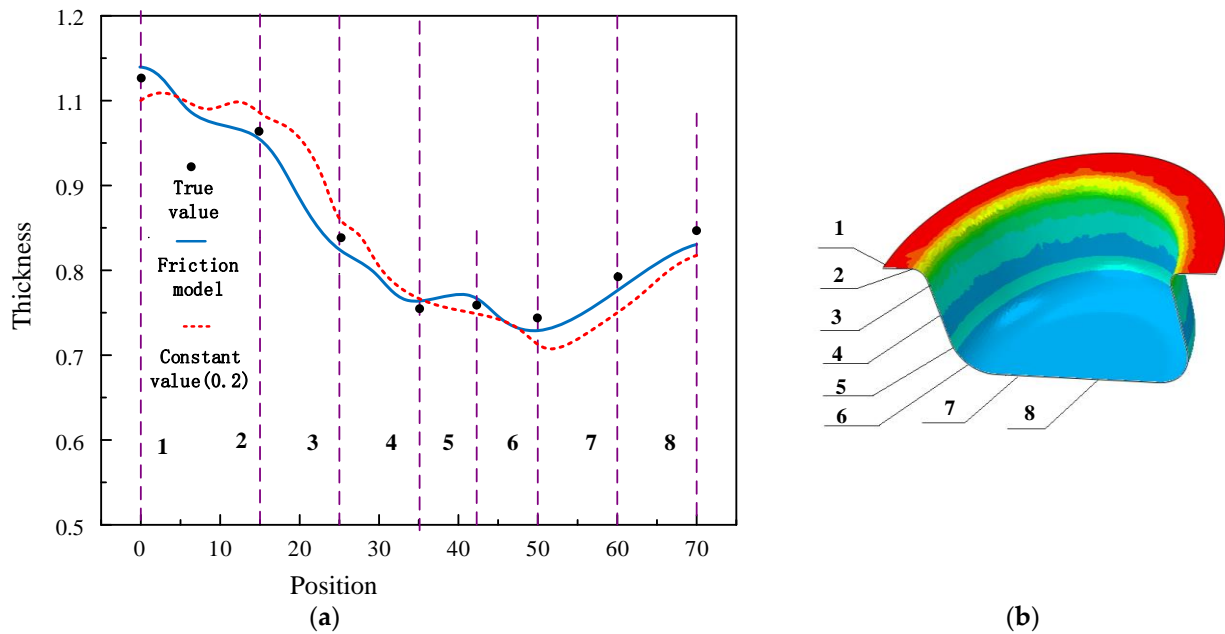
Figure 11. Wall thickness distribution at wall thickness position. (**a**) Wall thickness distribution s; (**b**) Wall thickness position.

Using the friction model, the blank shape is simulated and measured experimentally when the blank holder force is 10 kN and 30 KN, respectively. The blank shapes are compared, and the error is less than 5%. The comparison results show that the simulation and measurement results have a good agreement, as shown in Figure 12. The actual deep drawing of aluminum alloy and the cylinder after deep drawing in the verification experiment are shown in Figure 13.
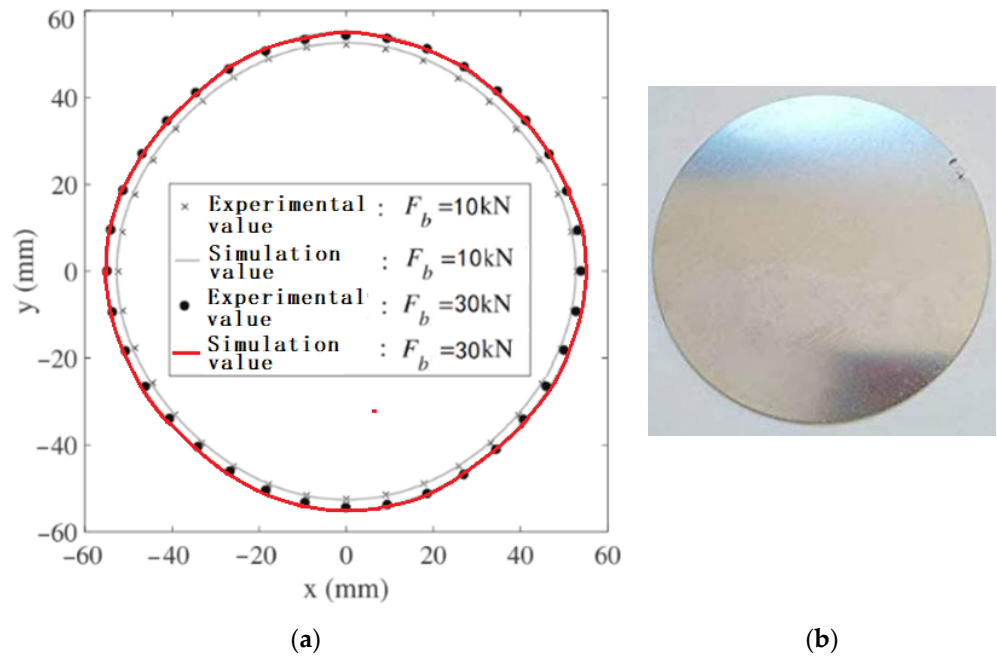
Figure 12. The blank shape of the part. (**a**) Blank sizes, (**b**) Real blank shape.

(**a**) (**b**)

Figure 13. Stamping test parts (**a**) Intact parts; (**b**) Cracked parts.

5. Conclusions

In this study, a new method for friction coefficient calculation in sheet metal forming is studied theoretically and experimentally. The theoretical model of friction coefficient calculation shows great significance and application value. The results are concluded as follows:

(1) A theoretical model using Coulomb friction coefficient measurement in metal sheet forming is established, and the solution algorithm of friction coefficient in deep drawing of symmetrical cylindrical parts provides a theoretical basis for the research of friction coefficient measurement methods.

(2) The friction coefficients for two types of plates under different lubrication conditions are calculated using MATLAB software and measured experimentally, which shows a good agreement. This method can be used as a standard measurement method of friction in the sheet metal stamping process.

(3) With the comparison of fixed friction coefficients in finite element simulation for the drawing process of symmetrical parts, the new friction coefficient models can improve the simulation accuracy.

(4) The application of the friction model can effectively improve the simulation accuracy of finite element software.

References

1. Dou, S.; Wang, X.; Xia, J.; Wilson, L. Analysis of Sheet Metal Forming (Warm Stamping Process): A Study of the Variable Friction Coefficient on 6111 Aluminum Alloy. *Metals* **2020**, *10*, 1189. [CrossRef]
2. You, K.; Kim, H.-K. A Study on the Effect of Process and Material Variables on the Hot Stamping Formability of Automotive Body Parts. *Metals* **2021**, *11*, 1029. [CrossRef]
3. Evin, E.; Daneshjo, N.; Mareš, A.; Tomáš, M.; Petrovčiková, K. Experimental Assessment of Friction Coefficient in Deep Drawing and Its Verification by Numerical Simulation. *Appl. Sci.* **2021**, *11*, 2756. [CrossRef]
4. Azushima, A.; Kudo, H. Direct Observation of Contact Behaviour to Interpret the Pressure Dependence of the Coefficient of Friction in Sheet Metal Forming. *CIRP Ann.* **1995**, 209–212. [CrossRef]

5.   Dohda, K.; Wang, Z. Effects of Average Lubricant Velocity and Sliding Velocity on Friction Behavior in Mild Steel Sheet Forming. *J. Tribol.* **1998**, *120*, 724–728. [CrossRef]
6.   Ma, N.; Sugitomo, N. Development and Application of Non-linear Friction Models for Metal Forming Simulation. *Conf. Proc.* **2011**, *1383*, 382–389. [CrossRef]
7.   Wilson, W.R.D.; Hsu, T.C.; Huang, X.B. A Realistic Friction Model for Computer Simulation of Sheet Metal Forming Processes. *J. Eng. Ind.* **1995**, *117*, 202–209. [CrossRef]
8.   Comstock, R.J., Jr.; Kaiping, L.; Wagoner, R.H. Simulation of axisymmetric sheet forming tests. *J. Mater. Processing Technol* **2001**, *117*, 153–168. [CrossRef]
9.   Hildenbrand, A.; Bretault, N.; Hashimoto, K. Non-Linear Friction Laws Friction Coefficient as a Function of Contact Parameters. *SAE Tech. Pap. Ser.* **2006**, *4*, 39–45. [CrossRef]
10. Hashimoto, K.; Isogai, E.; Yoshida, T.; Kuriyama, Y.; Ito, K. Finite element analysis of sheet metal forming taking account of nonlinear friction model-assessment of sheet formability by nonlinear friction model III. *J. JSTP.* **2008**, *49*, 995–999. [CrossRef]
11. Dohda, K.; Boher, C.; Rezai-Aria, F.; Mahayotsanun, N. Tribology in metal forming at elevated temperatures. *Friction* **2015**, *3*, 1–27. [CrossRef]
12. Bhushan, B.; Kulkarni, A.V. Effect of Normal Load on Microscale Friction Measurements. *Thin Solid Films* **1996**, *2678*, 293–333. [CrossRef]
13. Chowdhury, M.A.; Khalil, M.K.; Nuruzzaman, D.M.; Rahaman, M.L. The Effect of Sliding Speed and Normal Load on Friction and Wear Property of Aluminum. *J. Mec. Mechat. Eng.* **2012**, *11*, 1–11.
14. Ramezani, M.; Ripin, Z.M. Analysis of deep drawing of sheet metal using the Marform process. *Int. J. Adv. Manuf. Technol.* **2012**, *59*, 491–505. [CrossRef]
15. Hol, J.; Alfaro, M.V.C.; Rooij, M.B.D.; Meinders, T. Advanced friction modeling for sheet metal forming. *Key Eng. Mater.* **2012**, *286*, 66–78. [CrossRef]
16. Koyama, H.; Manabe, K.-I. Virtual processing in intelligent BHF control deep drawing. *J. Mater. Process. Technol.* **2003**, *143–144*, 261–265. [CrossRef]
17. Wang, C.; Ma, R.; Zhao, J. Calculation method and experimental study of coulomb friction coefficient in sheet metal forming. *J. Manuf. Process.* **2017**, *27*, 126–137. [CrossRef]